

RESEARCH ARTICLE

Study of Complementary Loop Integrated Metasurface for 6G THz Communication

MONISHA SELVARAJ¹, (Student Member, IEEE), RAMYA VIJAY¹, (Senior Member, IEEE),
RAJESH ANBAZHAGAN¹, (Senior Member, IEEE), C. V. RAVIKUMAR^{1,2},
GIOVANNI PAU³, (Senior Member, IEEE), SATHISH KUMAR²,
AND S. PRABU⁴, (Senior Member, IEEE)

¹School of Electrical and Electronics Engineering, SASTRA Deemed to be University, Thanjavur, Tamil Nadu 613401, India

²School of Electronics Engineering, Vellore Institute of Technology, Vellore 632014, India

³Department of Engineering and Architecture, Kore University of Enna, 94100 Enna, Italy

⁴Department of Banking Technology, Pondicherry University (A Central University), Puducherry 605014, India

Corresponding authors: Ramya Vijay (ramyavijay@ieee.org), Giovanni Pau (giovanni.pau@unikore.it), and Rajesh Anbazhagan (rajeshthece@gmail.com)

ABSTRACT This article investigates the complementary frequency selective surface based metasurface structure that operates at 0.82 THz frequency. Various metasurface structures with single and multi-layered substrates have been reported in literature for sixth generation systems. Here, we review various potential metasurface structures for THz communication. Moreover, a dual complementary loop integrated three-legged structure and related loop integrated metasurface has been studied. The complementary loop integrated is embossed on a polydimethylsiloxane substrate to achieve better angular stability over 0° to 85° with a maximum frequency deviation of 0.05%. The choice of substrate is also investigated with their flexibility and suitability for THz frequency. The equivalent circuit model we analyzed for complementary loop integrated and conventional approaches. The results depict that the complementary structure can achieve better angular stability over the incident angle of 0° to 85° for both TE and TM modes.

INDEX TERMS Angular stability, equivalent circuit model, frequency selective surface, loop structure, metasurface, THz communication.

I. INTRODUCTION

Recently, metasurface have attracted a significant deal of attention [1], [2], [3], [4], [5], [6], [7], [8], [9], [10]. Metasurface are innovative unreal materials with special features that are not typically present in nature. Initial instances of these were synthetic dielectrics in the setting of electromagnetics. The term “metasurface” refers to a periodic/apperiodic structure in which the dimension and periodicity of its specific components are comparatively small in relation to the operating wavelength. These 2-Dimensional structures can also be further subclassified as a reflecting screen with several apertures is referred to as a meta screen, and distinct individual scatterers are referred to as meta films [11]. However, the available literature has not typically supported this classification. In order to modulate the electromagnetic response

of the surface, metasurface can alternatively be thought of as an array of sub-wavelength resonant scatterers [12]. The arrangement of specific scatterers plays an important part in surface response. These characteristics discriminate the metasurface from conventional Frequency Selective Surface (FSS). And another way is that each component of a metasurface is sub-wavelength than conventional FSS are on the order of operating wavelength. The structure for metasurface can be thought of as traditional homogeneous structures because of their sub-wavelength nature, which makes it possible to characterize their reaction with useful parameters. The thin size of metasurface emphasis the presence of the angular stability and polarizations stability. Normally, the periodic array structure has the capability to change the performances of the Electromagnetic waves (EM). When the polarization or incident EM waves changes, the structure of the surface will show different performances. This is the most case should be considered for designing the FSS structure or any

The associate editor coordinating the review of this manuscript and approving it for publication was Wanchen Yang¹.

other array structures. In [13], an analytical strategy based on the reflection and transmission dualistic is presented. Using the electric and magnetic surface, general surface transition circumstances enable the composite distribution of the meta-elements to be changed with boundary conditions [14]. Using, this homogenization technique leaky-wave antennas [15]; fractal metasurface [16]; and non-linear metasurface [17] has been designed. It is important to note that aperiodic element arrangements have been used in reflect-array design. Each component is made to inform the correct phase shift to give a reflected beam the desired direction. In [18], [19], [20], and [21], some examples are shown. Each specific unit cell may be spatially changed because the metasurface sheet's reaction is supported on the limited performance of each unit [22].

In this study, the structures of metasurface and their performances will be covered. Generally, the structure of FSS can also be used to design the metasurface elements. According to Munk's idea, few FSS elements have different characteristics depends on the shape and structure of the elements. Further from the study of structure, the paper proceeds with unique simple layer transmitting FSS with greater angular stability and polarization insensitivity with the integration of loop and non-loop structure. The integration of loop and non-loop designs from different FSS groups facilitates the stable resonance frequency over a wide incident angle of 0° to 85° for both the modes of operations. In addition, the derived equivalent circuit model helps to understand the transmission mechanism of the proposed dual complementary loop integrated three-legged structure.









II. LITERATURE SURVEY

Basically, there are various array elements are used for metasurface designs. They are depending on basic element type, meander line structure and fractal structure. Firstly, structure based on element type contains groups of element structures and its performances are shown in Table 1.

Conventionally, the group 3 complementary planes [23] and circular ring patches [24] are used to attain the specific band frequencies in oblique angles of incidence. Generally, choosing a group 2 type of elements with a greater loop area is helpful and it improves the bandwidth [25]. Simple circular loops [26] and square loops [27] have been used to advance loaded elements with three or four legs [28]; hexagonal loop [29] designs are advantageous for wideband applications. FSS reaches the resonance when the circumference of the loop element approaches a whole wavelength. It has been discovered that altering the shape of these loop elements—loaded three- or four-legged components, which are narrow band, and hexagon loops, which are ultra-wideband—allows for the achievement of a wide range of bandwidth. For instances, Cross-folded element [30] and convoluted square loop [31] structure stabilize the FSS resonant frequency at any angle between 0° to 60° degrees.

Anchor-shaped and four-legged loop [32] elements also have better angular stability and dual-band performance [33].

TABLE 1. Performance metrics of various structures.

Groups	Structure	Performance
1		Three legged or tripod structure has three support legs to provide angular and structural stability [28]
		Anchor shaped structure helps to increase the bandwidth according to the applications [32]
		Square spiral structure helps to miniaturize the structure with higher electrical length [2]
2		Circular loop can be designed for light weight, low profile, high stable and operation requirements [26]
		Square loop designers can tailor the structure's frequency response to specific frequency bands of interest [27]
		Hexagonal loop can be employed for electromagnetic shielding to block specific frequency ranges while allowing others to pass. This is useful for mitigating electromagnetic interference (EMI) [29]
3		Square patch FSSs can improve the performance of radar and communication systems by reducing clutter, managing interference, and enhancing signal quality [23]
		The grid arrangement of circular patches allows for efficient space utilization, making them advantageous for applications with limited space availability [16]

The miniaturized loop element in [34] and [35] attains stable resonance frequency for WLAN applications for incident angles 0° to 60° . Still, the range of incident angles is not sufficient for some applications. For some applications demand miniaturized structure, for that meander line concept was initially invented. Due to this technique, electrical length can be increased with tiny structures [36]. Even though, it reduces the overall size of the structure also reduces the band coverage, frequency shifting with incident angle and complex analysis and modelling of the structure. Nowadays, fractal structures are preferred to design the iterative method structure for multi-band operations, compactness and also achieved operating frequency response.

There are various self-similarity structures [37] are used for many wideband applications. Another systematic method for improving angular performance is the multilayer technique. With compact FSS, two meandering wire resonators coupled together and separated by a thin substrate offer angular stability up to 80 degrees. [38]. A Three-dimensional (3-D) structure is a multilayer structure to obtain stable operating frequency responses for incident angles 0° to 85° . In [39], a 3D 4-legged loaded loop is projected to retain the operating

frequency constant. However, the multilayer structures [40] improves the angular stability performance, but it is a complex development process. This study process gives the knowledge of the periodic basic loop structures are simple for wide band applications, angular stability, and miniaturized structure. Here, we proceed the paper with combinations of structure to achieve the appropriate performance.

III. COMPLEMENTARY LOOP-BASED STRUCTURE AND ITS PERFORMANCE

According to the theory in [41], spacing between the elements and their structures affects the angular stability of the FSS. In common, huge spacing between the elements in FSS results in grating lobes, whereas small layout contributes stability in operating frequency with incident angles. Even though small design can expand the angular stability of FSSs, the effect is confined. As declared above, the loop element structure has good angular stability and is miniaturized in size than the other basic structures of the unit cell. Therefore, loop elements are used in FSS design to attain better angular stability.

Initially, we deliberately chose to design square loop metasurface because of their high level of customizability and substrate's electrical thickness be smaller than the wavelength at the resonant frequency for getting optimal functionality. This ensures that the substrate can induce spatially uniform fields, resulting in an invariant response to electromagnetic waves at oblique angles. Also, this allowed us to modify their properties to perform specific functions such as focusing, beam steering, or filtering. With the ability to adjust the geometry of the loops, these metasurface were tailored to meet our specific design requirements. Therefore, complementary square loop (CSL) elements are etched on a Polydimethylsiloxane (PDMS) with a thickness of $15\mu\text{m}$ shown in Fig. 1a.

Generally, the symmetric current distribution pattern is an essential factor in stabilizing the transmission behavior of the metasurface. This helps ensure that the transmitted waves exhibit consistent characteristics for all incident angles. To achieve this, we need to focus on minimizing any asymmetric effects that could lead to fluctuations in the transmission response. Thus, we propose a new structure that maximizes angular stability for the operating frequency. From the current distribution of Fig.1a, the CSL has a symmetric high current only at the edges of the structure. And Fig. 1b and 1c shows the s-parameter results of incident angles 0° to 85° with some frequency drifts.

To enhance the angular stability, higher deviation in resonant frequency and reduces the square loop limitations including a high coupling effect between elements due to its symmetric structural property. We employed a combined loop metasurface, which integrates the square loop and octagonal loop. This approach provides improved angular stability, reduced resonance frequency deviation, and lower coupling between elements compared to a traditional square loop metasurface, making it highly effective in wireless applications.

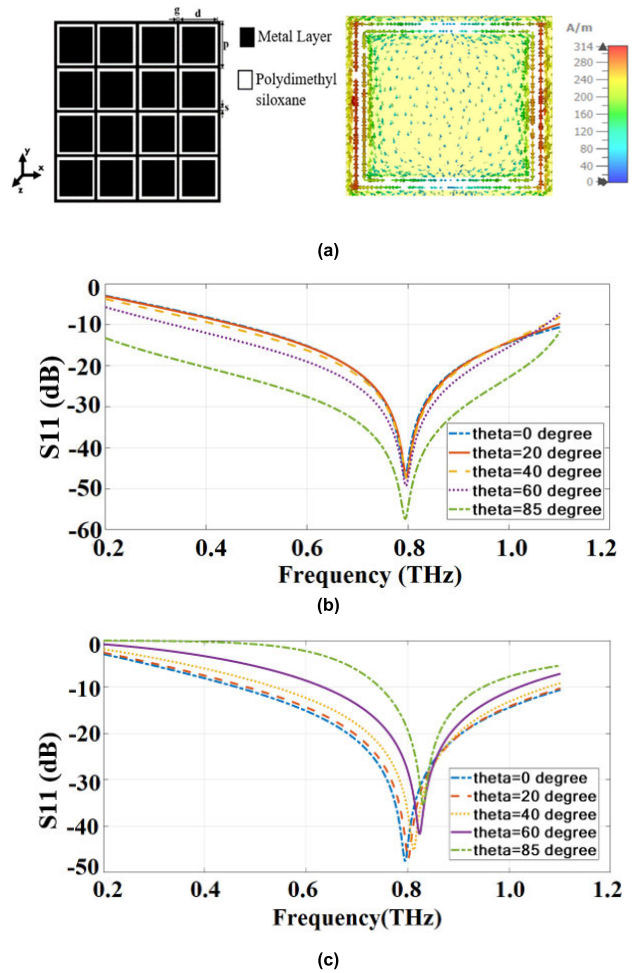


FIGURE 1. (a) Complementary square loop (CSL) structure and its current distribution of CSL Unit cell (b) Incident angle analysis of TE mode (c) Incident angle analysis of TM mode.

Normally, octagonal loop metasurface has ability to reduce coupling between neighboring elements and significantly enhancing the overall precision and performance of the metasurface. So, the octagonal loop is integrated with the CSL to form a dual complementary loop (DCL) structure and its current distribution provides a higher current distribution, especially at the edges of the structure shown in Fig. 2a., than the square loop metasurface. Fig. 2b and Fig. 2c shows the results in a stable resonance frequency at 0.82 THz with lesser frequency deviations (0.0084 THz and 0.0272 THz) when compared with CSL for both polarizations, as shown in figure 4. Our integrated loop structure ensured that electromagnetic waves transmitted from the source were polarized in a specific direction, resulting in significantly reduced signal degradation and improved overall transmission quality. Fig. 4 curve shows the stable resonance frequency at 0.82 THz with lesser frequency deviations (0.0084 THz and 0.0272 THz) when compared with CSL for both polarizations.

Also, we utilized three-legged metasurface at the center to adjust the phases and shapes of the transmitted waves,

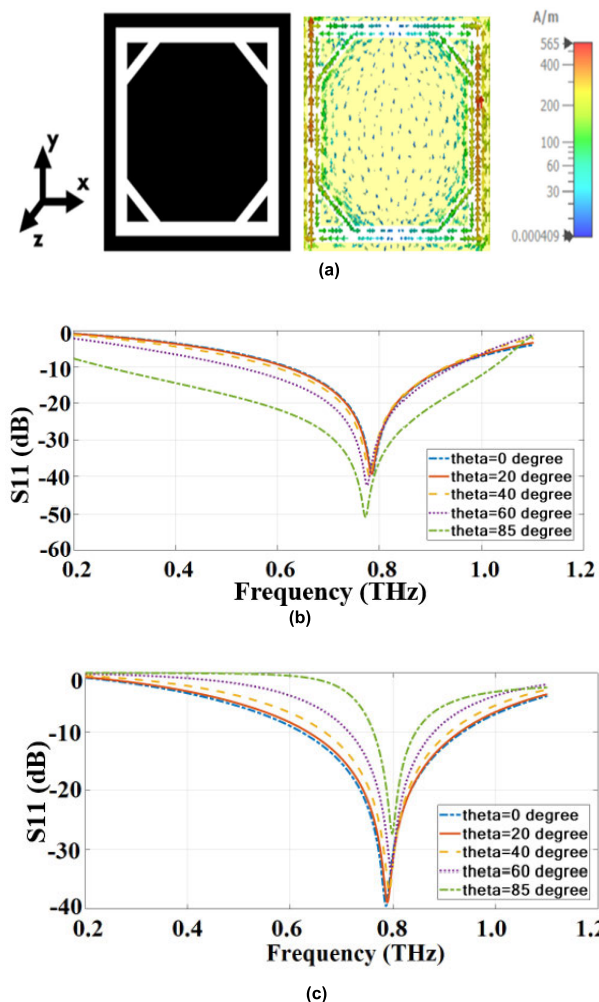


FIGURE 2. (a) Dual complementary loop (DCL) structure and its current distribution (b) Incident angle analysis of TE mode (c) Incident angle analysis of TM mode.

precisely steering them towards the intended receiver, even in the presence of obstacles or interference. The adjustable legs enable fine-tuning of the metasurface’s response to incident angles, ensuring stable and reliable performance across a wide range of viewing directions and incident angles.

Therefore, integrating the three-legged structure with DCL forms DCLITL, and its current distributions as shown in Fig. 3a, it represents a high symmetric current throughout the structure. A symmetric current distribution pattern in a proposed structure facilitates stable transmission behaviors by ensuring uniform phase control, minimizing unwanted scattering, and grating lobes, improving impedance matching, and enhancing predictability in wavefront manipulation. This symmetry contributes to robust performance, making the structure less sensitive to variations in incident conditions [49]. Additionally, the simplicity of symmetric designs aids in easier fabrication and integration, promoting consistent and reliable transmission properties for diverse

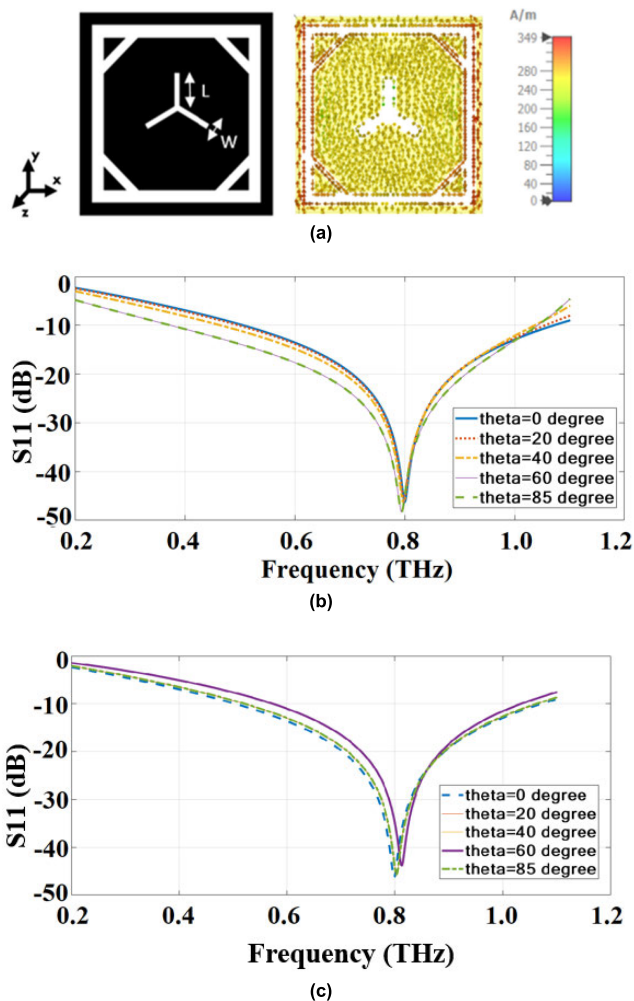


FIGURE 3. (a) Three-legged structure with OCSL and its current distribution (b) Incident angle analysis of TE mode (c) Incident angle analysis of TM mode.

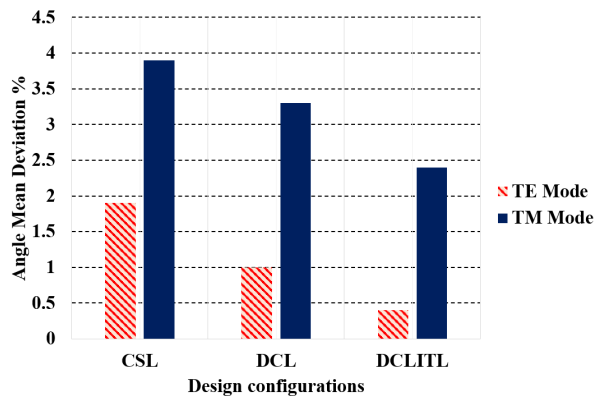


FIGURE 4. Angular mean deviation chart for different design configurations.

applications in electromagnetic wave manipulation. The three-legged structure with OCSL can obtain symmetric current distribution due to its closed-loop nature and three-legged structure has equal lengths and similar shapes for each leg,

TABLE 2. Dimensions of the proposed unit cell.

Parameter	d	S	L	p	G	g	W
Dimension (um)	85	15	19.42	100	5	15	2

ensuring that the currents experience similar conditions and interactions. This uniformity in the current distribution helps in achieving symmetric electromagnetic responses. The legs and loop interact in a way that promotes balanced current distribution throughout the structure. The etched slots create discontinuities in the metasurface, leading to changes in the distribution of surface currents. Currents may be concentrated around the edges of the slots [50]. Updating each configuration geometry of the metasurface can impact the distribution of electromagnetic currents. With the proposed DCLTIL structure, the angular stability maximizes with lower frequency deviations shown in Fig. 3b and Fig. 3c results. The maximum frequency deviation for DCLITL is 0.0036 THz and 0.02 THz for TE and TM cases, respectively, as shown in figure 4.

Here, the overall size of the unit cell (DCLITL) is maintained as CSL and OCSL. The micro dimensions of the DCLITL are listed in table 2.

The mean of frequency deviation from operating frequency of each incident angle variation is called as Angle Mean Deviation (AMD). The proper selection of the structure helps to reduce variations in resonance frequency at various incident angle. The Angle Mean Deviation (AMD) can be used to calculate the frequency deviation, and it can determine the angular stability for TE and TM modes of operation under varying incidence angles using (1) [51],

$$\delta f_{as} = \sum_{i=0}^n \frac{f_r^{normal} - f_r^{a_i}}{n f_r^{normal}} \times 100\% \quad (1)$$

where f_{as} , f_r^{normal} , $f_r^{a_i}$ and n are the deviation of the resonating frequency, resonating frequency at normal incidence angle, the resonating frequency at various incidence angles, and number incidence angle, respectively. Even though the metasurface structure itself is symmetric, the incident wave conditions may not be symmetric [49]. Though the proposed structure is symmetric, there is slight variation in frequency due to various incident angles (0° to 85°) at both TE and TM modes of polarizations.

IV. EQUIVALENT CIRCUIT MODEL FOR THE PROPOSED STRUCTURE UNITS

To analyze and validate the proposed structure, an analytical method such as the Equivalent Circuit Model (ECM) method helps to prove the design performances. This provides a simplified electrical representation of the metasurface structure. And the ECM for a metasurface is a simplified representation that captures the essential electrical properties of the structure. It allows us to analyze and understand the Meta

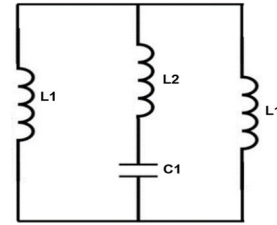


FIGURE 5. Equivalent circuit for CSL.

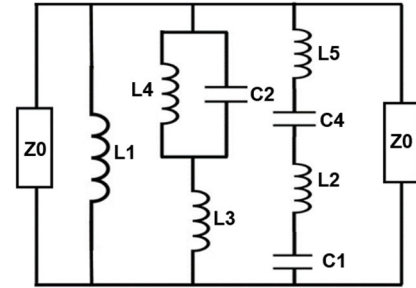


FIGURE 6. Equivalent circuit model for DCLITL.

surface's behavior in terms of electrical components [52]. The capacitor and inductor elements commonly used in metasurface modeling to explain the physical interpretation of the equivalent circuit model. Normally, capacitors represent the storage of electric charge. It can model the capacitance associated with the gaps or spaces between metallic elements. The capacitance influences the response of the metasurface to electromagnetic waves. Inductors in the equivalent circuit model represent the inductive behavior of the metasurface. This can arise from the loops or spiral structures within the unit cells. Inductive elements play a role in shaping the metasurface's response to varying electromagnetic fields.

According to this theory, the ECM for the proposed structure is construct. The capacitors are connected in the gap between the metallic elements and inductors are connected in the conducting spaces.

In [27], a conventional formula is specified to calculate the equivalent circuit elements of metal layers. The same formulas can be used to calculate the inductance and capacitance values of CSL. Using the basic formulas from (2) to (8), the equivalent circuit model for CSL is modelled with the combinations of inductors and capacitors shown in Fig.5.

$$L_1 = \frac{X_{L11}}{Z_0} = \cos \theta F(p, g, \lambda, \theta) \quad (2)$$

$$k = p - 2s, l = d - 2s \quad (3)$$

$$U = \frac{X_{L21}}{Z_0} = \frac{k}{p} \cos \theta F(p, l, \lambda, \theta) \quad (4)$$

$$L_2 = \frac{X_{L22}}{Z_0} = U + \frac{s}{l+g} L_1 \quad (5)$$

$$L = \frac{C_1}{Y_0} = 4 \sec \theta F(p, d, \lambda, \theta) \quad (6)$$

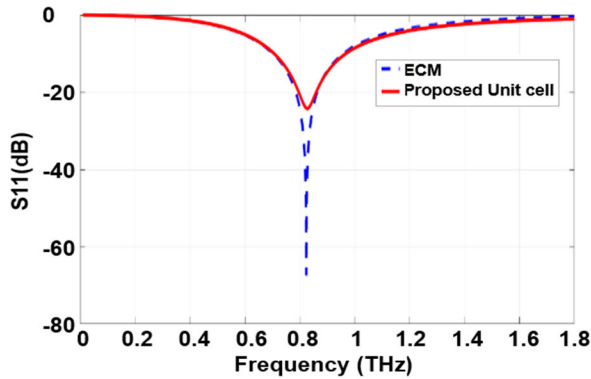


FIGURE 7. Comparison results of proposed structure with the equivalent circuit mode.

TABLE 3. Values of lumped elements of DCLITL.

Lumped Elements	L1	L2	L3	L4	L5	C1	C2	C3
Values	0.3 pH	0.75 pH	0.12 pH	1pH	0.5 pH	37 fF	16.8 fF	8f F

$$M = \frac{C_2}{Y_0} = 4 \sec \theta F(d - s, s, \lambda, \theta) \quad (7)$$

$$C_1 = \frac{C}{Y_0} = (1.75 L + 0.6 M) \epsilon_{eff} \quad (8)$$

In Equation.1, X_{L11} denotes the inductance of the outer square loop with width g . X_{L21} in 3 denotes the inductance of the inner square with l (2), which can be multiplied with k (2). Here, X_{L22} is an inductance influenced by 3. The capacitance value of the slotted square loop is attained from 5 (capacity between thickness g and length d) and 6 (capacitor between thickness g and inner square).

The value of the inductance and capacitance are $L1=0.3\text{pH}$, $L2=0.75\text{pH}$, $C1=37.8293\text{fF}$. By using CSL equivalent circuit, the CFSS (DCLITL) can be optimized, as shown in Fig. 6. The elements in the CFSS can be separated into two parts as capacitive part and the inductive part. For the various incident angles for both the polarization, the parts in the element with the E-field are said to be the inductive part, and the remaining part is the capacitive part. Considering [38], the capacitive and inductive parts achieve the capacitance C and inductance L , respectively. The L and C values can be calculated and tabulated for normal incident angles in Table 3. Further, the model has been designed using an EM simulation tool. Fig. 7 shows good agreement with the proposed structure and equivalent circuit model. Thus, the proposed work is mathematically proved that it works as transmission surface.

V. RESULTS AND DISCUSSIONS

Various analyses such as configuration, parameter, metasurface, and array analysis are performed to study the characteristics of proposed FSS structures. The analysis is explained in detail in the following paragraphs.

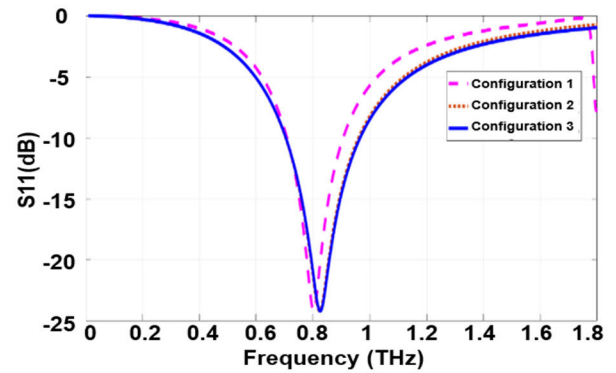
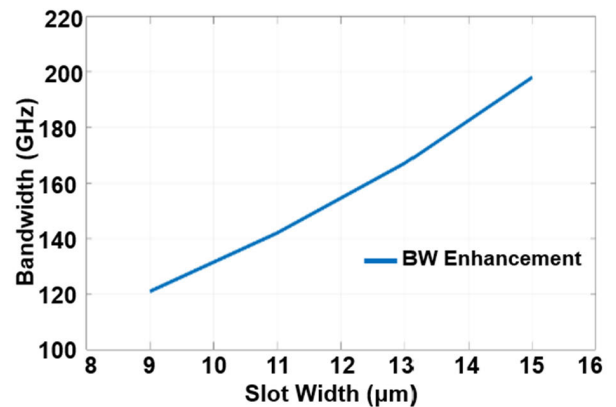
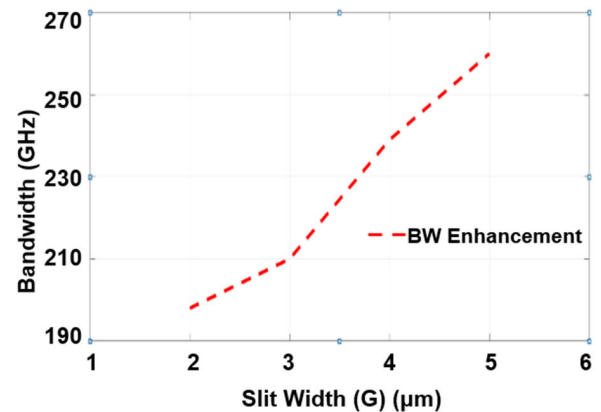


FIGURE 8. Comparison results of proposed structure with the equivalent circuit mode.



(a)



(b)

FIGURE 9. (a) Bandwidth enhancement vs. slot width (b) Bandwidth enhancement vs. G.

A. CHARACTERISTICS OF THE PROPOSED UNIT CELL

The reflection coefficients of the different configurations of the proposed unit cell are shown in Fig. 8. At various oblique incidence angles, the suggested DCLITL structure achieved a wider impedance bandwidth of 23.08 % than the CSL and higher angular stability and polarization insensitivity.

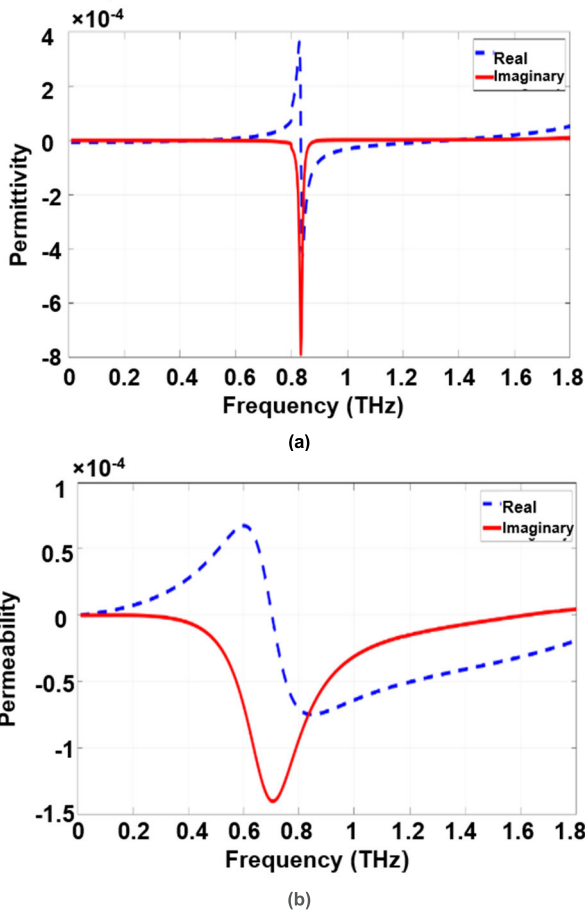


FIGURE 10. (a) Effective permittivity (b) Effective Permeability.

B. PARAMETERS' INFLUENCE ON UNIT CELL ANALYSIS

The shape of FSS allows for modification of both its operating frequency and operational bandwidth. As a result, the effects of altering the outer square loop's width and the CSL's G value have been investigated. Fig. 9(a-b) displays the bandwidth improvement for various square slot width dimensions and G. The resonating wavelength is set to be almost exactly equal to the loop's perimeter. This study reveals the connection between loop diameter and impedance bandwidth.

C. METASURFACE ANALYSIS

Effective permeability and permittivity's amplitudes are shown in Figs. 10a and 10b, respectively. The frequency response at 0.8 GHz has negative peaks in the effective medium. From 0.7 THz, the permeability curve in Fig. 12b produces negative actual values. The suggested meta-surface has left-handed properties because it possesses negative permeability and permittivity at 0.8 THz.

D. S-PARAMETER ANALYSIS ON ARRAY SIZE

Due to metasurface characteristics, the array size (Fig. 11) increases operating frequency is approximately the same. Fig 12. curve shows the S-parameter analysis for 2 × 2,

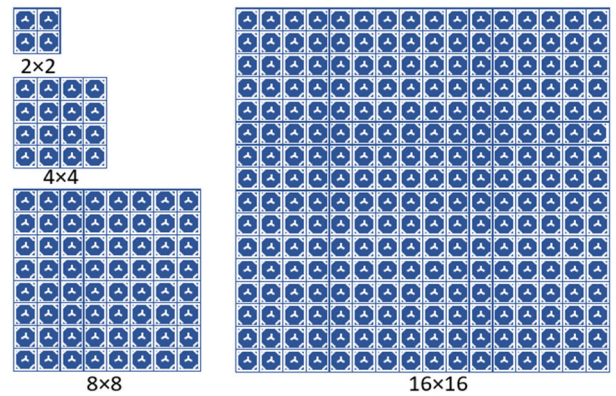


FIGURE 11. Shows the various array geometry of the proposed structure.

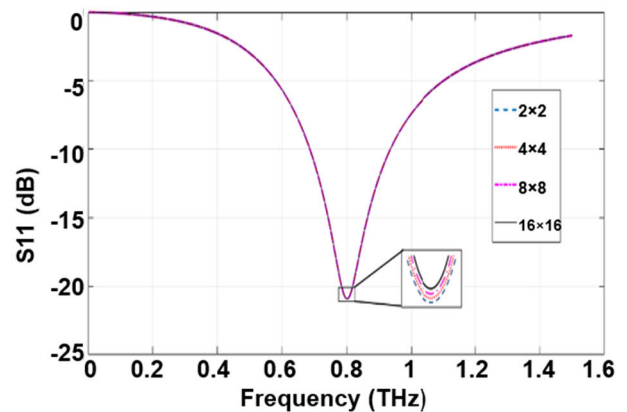


FIGURE 12. S-Parameter analysis of array.

4 × 4, 8 × 8, and 16 × 16. The arrangement and spacing of meta-atoms influence the impedance matching of the metasurface [53]. So, the proposed structure has little influence on the performances of array geometry. The proposed metasurface resonates with a stable operating frequency of 0.82 THz while increasing the array size.

To the author's knowledge, single layer high angularly stable transmitted metasurface were not available at THz frequency. So, Table 4. demonstrates a comparative study of existing structures [43], [44], [45], [46], [47], [48] with the proposed DCLITL structure irrespective of functionality. The parameters considered for the performance comparison are the angular stability at TE and TM mode, Bandwidth, and design configurations of the structures. The meta square ring design and fractal design gave up to 60° the angular stability for both the modes above. The square patch structures could provide up to 60° angular stability but not for both modes of operations. And papers [34], [35] provides up to 50° of angular stability with multi-layer structures. The proposed DCLITL gives up to 85° the angular stability with a 0.05% maximum deviation. This could be achieved by combining a dual complementary loop structure with a three-legged (non-loop) design. The achieved range of angular stability evidence

TABLE 4. Comparison between the existing structure and proposed structure.

Ref.	Structure Type	Bandwidth (THz)	Angular Stability		Design Configuration
			TE Mode	TM Mode	
This Work	Dual complementary loop integrated three-legged (DCLITL) Metasurface	0.72-0.98	85°	85°	Single Layer
[43]	Meta Square Ring	2.2-4.6	60°	60°	Single Layer
[44]	Disk and Square Ribbon	1.482-3.655	30°	30°	Single Layer
[45]	Square Patch	0.86-3.54	45°	65°	Multi-Layer
[46]	Square, Cross, and Circular shaped metasurface	0.55-3.12	40°	50°	Multi-Layer
[47]	Windmill structure	2.54-3.70	50°	50°	Multi-Layer
[48]	Fractal design	5.94 GHz	60°	60°	Multi-Layer

the suitability of DCLITL as a base for future high-frequency antenna radomes for better control of transmitted electromagnetic waves.

VI. CONCLUSION

Our article investigates the dual complementary loop integrated three-legged metasurface structure that operates at 0.82 THz and has a wider impedance bandwidth of 260 GHz. Throughout our study, we observed a maximum deviation of only 0.05% on the frequency of operation for the entire angle of incidence from 0° to 85°. Our analysis of the metasurface confirms that it is expandable to any sized array and can be used as a reflecting surface. In this paper, we conducted a comprehensive analysis in this work and presented our findings. However, the DCLITL structure has angular stability over a wide-angle, wide impedance bandwidth, and compact structure, making it a viable option for future high-frequency antenna radomes. It allows for better control of transmitted electromagnetic waves and can be used for beam steering applications.

REFERENCES

- [1] C. L. Holloway, E. F. Kuester, J. A. Gordon, J. O'Hara, J. Booth, and D. R. Smith, "An overview of the theory and applications of metasurfaces: The two-dimensional equivalents of metamaterials," *IEEE Antennas Propag. Mag.*, vol. 54, no. 2, pp. 10–35, Apr. 2012, doi: [10.1109/MAP.2012.6230714](https://doi.org/10.1109/MAP.2012.6230714).
- [2] S. S. Bukhari, J. Vardaxoglou, and W. Whitrow, "A metasurfaces review: Definitions and applications," *Appl. Sci.*, vol. 9, no. 13, p. 2727, Jul. 2019, doi: [10.3390/app9132727](https://doi.org/10.3390/app9132727).
- [3] N. Yu and F. Capasso, "Flat optics with designer metasurfaces," *Nature Mater.*, vol. 13, no. 2, pp. 139–150, Jan. 2014, doi: [10.1038/nmat3839](https://doi.org/10.1038/nmat3839).
- [4] G. Yoon, I. Kim, and J. Rho, "Challenges in fabrication towards realization of practical metamaterials," *Microelectron. Eng.*, vol. 163, pp. 7–20, Sep. 2016, doi: [10.1016/j.mee.2016.05.005](https://doi.org/10.1016/j.mee.2016.05.005).
- [5] C. M. Soukoulis and M. Wegener, "Past achievements and future challenges in the development of three-dimensional photonic metamaterials," *Nature Photon.*, vol. 5, no. 9, pp. 523–530, Jul. 2011, doi: [10.1038/nphoton.2011.154](https://doi.org/10.1038/nphoton.2011.154).
- [6] N. Meinzer, W. L. Barnes, and I. R. Hooper, "Plasmonic meta-atoms and metasurfaces," *Nature Photon.*, vol. 8, no. 12, pp. 889–898, Nov. 2014, doi: [10.1038/nphoton.2014.247](https://doi.org/10.1038/nphoton.2014.247).
- [7] A. V. Kildishev, A. Boltasseva, and V. M. Shalaev, "Planar photonics with metasurfaces," *Science*, vol. 339, no. 6125, pp. 12320091–12320096, Mar. 2013, doi: [10.1126/science.1232009](https://doi.org/10.1126/science.1232009).
- [8] Z. H. Jiang, S. Yun, L. Lin, J. A. Bossard, D. H. Werner, and T. S. Mayer, "Tailoring dispersion for broadband low-loss optical metamaterials using deep-subwavelength inclusions," *Sci. Rep.*, vol. 3, no. 1, pp. 1–9, Mar. 2013, doi: [10.1038/srep01571](https://doi.org/10.1038/srep01571).
- [9] M. Albooyeh, C. Simovski, and S. Tretyakov, "Homogenization and characterization of metasurfaces: General framework," in *Proc. 10th Eur. Conf. Antennas Propag. (EuCAP)*, Apr. 2016, pp. 1–3, doi: [10.1109/EuCAP.2016.7481662](https://doi.org/10.1109/EuCAP.2016.7481662).
- [10] C. L. Holloway and E. F. Kuester, "A homogenization technique for obtaining generalized sheet-transition conditions for a metafilm embedded in a magnetodielectric interface," *IEEE Trans. Antennas Propag.*, vol. 64, no. 11, pp. 4671–4686, Nov. 2016, doi: [10.1109/TAP.2016.2600764](https://doi.org/10.1109/TAP.2016.2600764).
- [11] C. L. Holloway, A. Dienstfrey, E. F. Kuester, J. F. O'Hara, A. K. Azad, and A. J. Taylor, "A discussion on the interpretation and characterization of metafilms/metamaterials: The two-dimensional equivalent of metamaterials," *Metamaterials*, vol. 3, no. 2, pp. 100–112, Oct. 2009.
- [12] A. Díaz-Rubio and S. A. Tretyakov, "Acoustic metasurfaces for scattering-free anomalous reflection and refraction," *Phys. Rev. B, Condens. Matter*, vol. 96, no. 12, Sep. 2017, Art. no. 125409, doi: [10.1103/physrevb.96.125409](https://doi.org/10.1103/physrevb.96.125409).
- [13] N. Shlezinger, G. C. Alexandropoulos, M. F. Imani, Y. C. Eldar, and D. R. Smith, "Dynamic metasurface antennas for 6G extreme massive MIMO communications," *IEEE Wireless Commun.*, vol. 28, no. 2, pp. 106–113, Apr. 2021, doi: [10.1109/MWC.001.2000267](https://doi.org/10.1109/MWC.001.2000267).
- [14] G. Minatti, M. Faenzi, E. Martini, F. Caminita, P. De Vita, D. González-Ovejero, M. Sabbadini, and S. Maci, "Modulated metasurface antennas for space: Synthesis, analysis and realizations," *IEEE Trans. Antennas Propag.*, vol. 63, no. 4, pp. 1288–1300, Apr. 2015, doi: [10.1109/TAP.2014.2377718](https://doi.org/10.1109/TAP.2014.2377718).
- [15] F. Mesa, G. Valerio, R. Rodríguez-Berral, and O. Quevedo-Teruel, "Simulation-assisted efficient computation of the dispersion diagram of periodic structures: A comprehensive overview with applications to filters, leaky-wave antennas and metasurfaces," *IEEE Antennas Propag. Mag.*, vol. 63, no. 5, pp. 33–45, Oct. 2021, doi: [10.1109/MAP.2020.3003210](https://doi.org/10.1109/MAP.2020.3003210).
- [16] T. Cai, G.-M. Wang, X.-F. Zhang, and J.-P. Shi, "Low-profile compact circularly-polarized antenna based on fractal metasurface and fractal resonator," *IEEE Antennas Wireless Propag. Lett.*, vol. 14, pp. 1072–1076, 2015, doi: [10.1109/LAWP.2015.2394452](https://doi.org/10.1109/LAWP.2015.2394452).
- [17] T. Huang, X. Zhao, S. Zeng, A. Crunteanu, P. P. Shum, and N. Yu, "Planar nonlinear metasurface optics and their applications," *Rep. Prog. Phys.*, vol. 83, no. 12, Nov. 2020, Art. no. 126101, doi: [10.1088/1361-6633/abb56e](https://doi.org/10.1088/1361-6633/abb56e).
- [18] G. Kim, S. Kim, H. Kim, J. Lee, T. Badloe, and J. Rho, "Metasurface-empowered spectral and spatial light modulation for disruptive holographic displays," *Nanoscale*, vol. 14, no. 12, pp. 4380–4410, Mar. 2022, doi: [10.1039/d1nr07909c](https://doi.org/10.1039/d1nr07909c).

- [19] M. K. T. Al-Nuaimi, W. Hong, and W. G. Whittow, "Nature-inspired orbital angular momentum beam generator using aperiodic metasurface," *J. Phys. D, Appl. Phys.*, vol. 54, no. 27, Apr. 2021, Art. no. 275106, doi: 10.1088/1361-6463/abe81f.
- [20] Majorel, C. Girard, A. Arbouet, O. L. Muskens, and P. R. Wiecha, "Deep learning enabled strategies for modeling of complex aperiodic plasmonic metasurfaces of arbitrary size," *ACS Photon.*, vol. 9, no. 2, pp. 575–585, Feb. 2022, doi: 10.1021/acsp Photonics.1c01556.
- [21] N. Chamok, M. Ali, T. Anthony, and S. J. Weiss, "Ultra-thin UHF broadband antenna on a non-uniform aperiodic (NUA) MetaSurface," *IEEE Antennas Propag. Mag.*, vol. 57, no. 2, pp. 167–180, Apr. 2015, doi: 10.1109/MAP.2015.2414491.
- [22] Z.-L. Xu, D.-F. Wang, Y.-F. Shi, Z.-H. Qian, B. Assouar, and K.-C. Chuang, "Arbitrary wavefront modulation utilizing an aperiodic elastic metasurface," *Int. J. Mech. Sci.*, vol. 255, Oct. 2023, Art. no. 108460, doi: 10.1016/j.ijmecs.2023.108460.
- [23] E. Zanganeh, M. Fallah, A. Abdolali, and N. Komjani, "New approach to design dual-band frequency selective surface based on frequency response tuning of each individual layer," *Microw. Opt. Technol. Lett.*, vol. 58, no. 6, pp. 1423–1429, Jun. 2016, doi: 10.1002/mop.29837.
- [24] X. Yao, M. Bai, and J. Miao, "Equivalent circuit method for analyzing frequency selective surface with ring patch in oblique angles of incidence," *IEEE Antennas Wireless Propag. Lett.*, vol. 10, pp. 820–823, 2011, doi: 10.1109/LAWP.2011.2164774.
- [25] I. Martinez, A. H. Panaretos, D. H. Werner, G. Oliveri, and A. Massa, "Ultra-thin reconfigurable electromagnetic metasurface absorbers," in *Proc. 7th Eur. Conf. Antennas Propag. (EuCAP)*, Gothenburg, Sweden, Apr. 2013, pp. 1843–1847.
- [26] A. Ramezani Varkani, Z. Hossein Firouzeh, and A. Zeidaabadi Nezhad, "Equivalent circuit model for array of circular loop FSS structures at oblique angles of incidence," *IET Microw., Antennas Propag.*, vol. 12, no. 5, pp. 749–755, Apr. 2018, doi: 10.1049/iet-map.2017.1004.
- [27] D. Ferreira, R. F. S. Caldeirinha, I. Cuiñas, and T. R. Fernandes, "Square loop and slot frequency selective surfaces study for equivalent circuit model optimization," *IEEE Trans. Antennas Propag.*, vol. 63, no. 9, pp. 3947–3955, Sep. 2015, doi: 10.1109/TAP.2015.2444420.
- [28] M. Khosravi and M. S. Abrishamian, "Reduction of monostatic RCS by switchable FSS elements," *PIERS Online*, vol. 3, no. 6, pp. 770–773, 2007, doi: 10.2529/piers061005040306.
- [29] S. N. Zabiri, R. Cahill, and A. Schuchinsky, "Compact FSS absorber design using resistively loaded quadruple hexagonal loops for bandwidth enhancement," *Electron. Lett.*, vol. 51, no. 2, pp. 162–164, Jan. 2015, doi: 10.1049/el.2014.3866.
- [30] R. Natarajan, M. Kanagasabai, S. Baisakhiya, R. Sivasamy, S. Palaniswamy, and J. K. Pakkathillam, "A compact frequency selective surface with stable response for WLAN applications," *IEEE Antennas Wireless Propag. Lett.*, vol. 12, pp. 718–720, 2013, doi: 10.1109/LAWP.2013.2264837.
- [31] M. Nauman, R. Saleem, A. K. Rashid, and M. F. Shafique, "A miniaturized flexible frequency selective surface for X-band applications," *IEEE Trans. Electromagn. Compat.*, vol. 58, no. 2, pp. 419–428, Apr. 2016, doi: 10.1109/TEMC.2015.2508503.
- [32] I. G. Lee and I. P. Hong, "3D frequency selective surface for stable angle of incidence," *Electron. Lett.*, vol. 50, no. 6, pp. 423–424, Mar. 2014, doi: 10.1049/el.2014.0053.
- [33] J. Y. Yin, X. Wan, J. Ren, and T. J. Cui, "A circular polarizer with beamforming feature based on frequency selective surfaces," *Sci. Rep.*, vol. 7, no. 1, pp. 1–10, Jan. 2017, doi: 10.1038/srep41505.
- [34] Z. Zhao, H. Shi, J. Guo, W. Li, and A. Zhang, "Stopband frequency selective surface with ultra-large angle of incidence," *IEEE Antennas Wireless Propag. Lett.*, vol. 16, pp. 553–556, 2017, doi: 10.1109/LAWP.2016.2588528.
- [35] M. Tang, D.-F. Zhou, Q.-K. Liu, Z.-N. Yao, and Q. Liu, "Low-profile FSS-based polarization-insensitive absorber with switchable transmission band," *IEEE Antennas Wireless Propag. Lett.*, vol. 20, pp. 1038–1042, 2021, doi: 10.1109/LAWP.2021.3070148.
- [36] Q. Li, S. Liu, X. Zhang, S. Wang, and T. Chen, "Electromagnetically induced transparency in terahertz metasurface composed of meanderline and U-shaped resonators," *Opt. Exp.*, vol. 28, no. 6, p. 8792, Mar. 2020, doi: 10.1364/oe.389292.
- [37] Y.-M. Yu, C.-N. Chiu, Y.-P. Chiou, and T.-L. Wu, "A novel 2.5-dimensional ultraminiaturized-element frequency selective surface," *IEEE Trans. Antennas Propag.*, vol. 62, no. 7, pp. 3657–3663, Jul. 2014, doi: 10.1109/TAP.2014.2321153.
- [38] T. Hong, W. Xing, Q. Zhao, Y. Gu, and S. Gong, "Single-layer frequency selective surface with angular stability property," *IEEE Antennas Wireless Propag. Lett.*, vol. 17, pp. 547–550, 2018, doi: 10.1109/LAWP.2018.2801864.
- [39] Y. Liang, M. Chen, Y. Zhou, L. Peng, Z. Li, and L. Dai, "A wide-band multilayer tunable filter using active frequency selective surface," *Microw. Opt. Technol. Lett.*, vol. 64, no. 1, pp. 83–89, Jan. 2022, doi: 10.1002/mop.33052.
- [40] P. Wang, Y. Wang, Y. Hu, H. Zhou, Z. Yan, and J. Ai, "Ultra-wideband and low-loss linear-to-circular polarizer based on multilayer frequency selective surface," *Appl. Phys. A, Solids Surf.*, vol. 127, no. 2, p. 103, Feb. 2021, doi: 10.1007/s00339-020-04263-1.
- [41] A. B. Munk, *Frequency Selective Surfaces: Theory and Design*. Hoboken, NJ, USA: Wiley, 2005.
- [42] H. Hsiao, C. H. Chu, and D. P. Tsai, "Fundamentals and applications of metasurfaces," *Small Methods*, vol. 1, no. 4, Apr. 2017, Art. no. 1600064.
- [43] S. Zakir, R. M. H. Bilal, M. A. Naveed, M. A. Baqir, M. U. A. Khan, M. M. Ali, M. A. Saeed, M. Q. Mehmood, and Y. Massoud, "Polarization-insensitive, broadband, and tunable terahertz absorber using slotted-square graphene meta-rings," *IEEE Photon. J.*, vol. 15, no. 1, pp. 1–8, Feb. 2023, doi: 10.1109/JPHOT.2022.3229900.
- [44] A. Norouzi-Razani and P. Rezaei, "Broadband polarization insensitive and tunable terahertz metamaterial perfect absorber based on the graphene disk and square ribbon," *Micro Nanostruct.*, vol. 163, Mar. 2022, Art. no. 107153.
- [45] X. Huang, M. Cao, D. Wang, X. Li, J. Fan, and X. Li, "Broadband polarization-insensitive and oblique-incidence terahertz metamaterial absorber with multi-layered graphene," *Opt. Mater. Exp.*, vol. 12, no. 2, p. 811, 2022.
- [46] M. Rahmzadeh, H. Rajabalipanah, and A. Abdolali, "Multilayer graphene-based metasurfaces: Robust design method for extremely broadband, wide-angle, and polarization-insensitive terahertz absorbers," *Appl. Opt.*, vol. 57, no. 4, p. 959, Feb. 2018, doi: 10.1364/ao.57.000959.
- [47] J. Xu, Z. Qin, M. Chen, Y. Cheng, H. Liu, R. Xu, C. Teng, S. Deng, H. Deng, H. Yang, S. Qu, and L. Yuan, "Broadband tunable perfect absorber with high absorptivity based on double layer graphene," *Opt. Mater. Exp.*, vol. 11, no. 10, p. 3398, 2021, doi: 10.1364/ome.439348.
- [48] T. Xie, D. Chen, H. Yang, Y. Xu, Z. Zhang, and J. Yang, "Tunable broadband terahertz waveband absorbers based on fractal technology of graphene metamaterial," *Nanomaterials*, vol. 11, no. 2, p. 269, Jan. 2021, doi: 10.3390/nano11020269.
- [49] C. Ni, X. Xie, and L. Zhang, "Research on the element structure and surface current distribution of metasurface based on characteristic mode analysis," *J. Appl. Phys.*, vol. 134, no. 18, Nov. 2023, doi: 10.1063/5.0174009.
- [50] T. A. Ndukaife and S. Yang, "Slot driven dielectric electromagnetically induced transparency metasurface," *Opt. Exp.*, vol. 31, no. 17, p. 27324, 2023, doi: 10.1364/oe.488704.
- [51] M. Selvaraj, R. Vijay, R. Anbazhagan, and A. Rengarajan, "Reconfigurable metasurface: Enabling tunable reflection in 6G wireless communications," *Sensors*, vol. 23, no. 22, p. 9166, Nov. 2023, doi: 10.3390/s23229166.
- [52] X. Chen, C. An, J. Zhou, and W. Li, "Independent wavefront manipulation of broadband spin-decoupled metasurfaces based on equivalent circuit model," *Phys. Scripta*, vol. 98, no. 9, Sep. 2023, Art. no. 095518.
- [53] Y. Ma, J. F. Kolb, A. A. Ihalage, A. S. Andy, and Y. Hao, "Incorporating meta-atom interactions in rapid optimization of large-scale disordered metasurfaces based on deep interactive learning," *Adv. Photon. Res.*, vol. 4, no. 4, Apr. 2023, Art. no. 2200099.



MONISHA SELVARAJ (Student Member, IEEE) is currently pursuing the Ph.D. degree in RF and microwave with SASTRA Deemed to be University, India. Her research interests include frequency selective surface, intelligent reflecting surface, MIMO antennas, 3F antenna designs, phased array antennas, multiband antennas, spiral antenna, and antenna measurements. Experienced in a network analyzer and signal analyzer.



RAMYA VIJAY (Senior Member, IEEE) received the Ph.D. degree in multiband integrated antenna from SRM University, India, in 2017. Since completing the Ph.D. research, she has continued her research interests include RFID, smart antennas for vehicular communications, MIMO antennas, electromagnetic bandgap structure (EBG) assisted RF devices, planar phased array antennas, broadband microstrip antennas and arrays, beam-forming networks, and near-field/far-field antenna measurements. She has published around 25 papers in peer-reviewed international journals and international conference proceedings. She has hands-on experience with real-time propagation analysis, network analyzer, and signal analyzer. She is strong in multiband antennas, circular polarization concepts, integration of antennas with RF circuit, backscattered RFID and retransmission concepts, and AI. She is a member of IET and ISTE and an Associate Member of BES. She serving as a Treasurer for the IEEE AP-S Madras Section since 2019. She is also a iDex DISC 6 Challenge Winner. She has been awarded the “Young Women Researcher Award” by Science Father.



GIOVANNI PAU (Senior Member, IEEE) received the bachelor's degree in telematic engineering from the University of Catania, Italy, and the master's (cum laude) and Ph.D. degrees in telematic engineering from the Kore University of Enna, Italy. He is currently an Associate Professor with the Faculty of Engineering and Architecture, Kore University of Enna. He is the author/coauthor of more than 130 refereed papers published in journals and conference proceedings. His research interests include wireless sensor networks, fuzzy logic controllers, intelligent transportation systems, the Internet of Things, smart homes, and network security. He has been involved in several international conferences as the session co-chair and a technical program committee member. He serves/served as a leading guest editor in special issues of several international journals. He is an Editorial Board Member and an Associate Editor of several journals, such as IEEE ACCESS, *Wireless Networks* (Springer), *EURASIP Journal on Wireless Communications and Networking* (Springer), *Wireless Communications and Mobile Computing* (Hindawi), *Sensors* (MDPI), and *Future Internet* (MDPI).



RAJESH ANBAZHAGAN (Senior Member, IEEE) received the B.Tech. and M.Tech. degrees in electronics and communication engineering from Pondicherry University, in 2005 and 2008, respectively, and the Ph.D. degree from the Department of Electronics Engineering, School of Engineering and Technology, Pondicherry University, in 2014. He was with Indian Telephone Industries (Government of India), from 2005 to 2006, with Tata Consultancy Services, from 2008 to 2009, and VIT University, Vellore, from 2014 to 2020. He was a recipient of a Gold Medal at the PG Level from Pondicherry University and Pondicherry Engineering College. He has been awarded Innovation in Science Pursuit for Inspired Research (INSPIRE) Fellowship under assured Opportunity for Research Career (AORC) from the Department of Science and Technology (DST), Ministry of Science and Technology (MST), Government of India. He was awarded by Google to perform foundational data, machine learning (ML), and artificial intelligence (AI) tasks and build secure networks. He is currently an Associate Professor with the School of Electrical and Electronics Engineering, SASTRA Deemed University, Thanjavur. His current research interests include 5G/6G networks, the IoT (Industrial and Medical), MIMO antennas, photonic crystal, localization of UAV and sensor networks, and emerging wireless networks.



SATHISH KUMAR received the master's degree in communication systems from Jawaharlal Nehru Technology University, Anantapur, India, in 2017. He is currently a Research Scholar with the School of Electronics Engineering, Vellore Institute of Technology, Vellore, Tamil Nadu, India. His research interests include underwater wireless sensor networks, 5G communications, machine learning, and artificial intelligence.



C. V. RAVIKUMAR received the M.Tech. degree in digital electronics and communication system from Jawaharlal Nehru Technology University, Anantapur, in 2009, and the Ph.D. degree in communication networks from Vellore Institute of Technology (VIT), Vellore, India, in 2018. He is currently an Associate Professor with the Department of Embedded Technology, School of Electronics Engineering, VIT. His current research interests include communication networks, machine learning, deep learning, wireless sensor networks, and information security.



S. PRABU (Senior Member, IEEE) received the B.Eng. degree in CSE and the double M.Tech. and Ph.D. degrees in remote sensing and in CSE. He is currently a Certified Blockchain Associate. He was a Postdoctoral Fellow with the Department of Computer Science and Engineering, IIT Bombay. He guided eight Ph.D.'s and one M.S. (by Research). Acquired research grants worth 2.4 Cr. He has more than 130 publications in peer-reviewed journals and conferences, edited four books, published 16 book chapters, and one patent. He has organized three international conferences which include one IEEE conference as the chair and also participated in many workshops and seminars. He is a member of many professional bodies. He is having more than 19 years of experience in teaching and research. He was a Professor and the Head of the Department of Information Security, School of Computer Science and Engineering, VIT Vellore. Currently, he is an Associate Professor with the Department of Banking Technology, Pondicherry University (A Central University), Puducherry, India.

...

Open Access funding provided by "Università degli Studi di Enna "KORE"" within the CRUI CARE Agreement